Получение, структура, свойства

UDC 548.57

Q. Liang, Y. F. Meng, C.-S. Yan, S. Krasnicki, J. Lai,
K. Hemawan, H. Shu (Washington, USA)
D. Popov (Argonne, USA)
T. Yu (Washington, USA)
W. Yang (Argonne, USA)
H. K. Mao, R. J. Hemley (Washington, USA)

Developments in synthesis, characterization, and application of large, high-quality CVD single crystal diamond

Single crystal diamond synthesis by microwave plasma chemical vapor deposition at rapid growth rate has considerably advanced in the past few years. Developments have been made in growth, optical quality, and mechanical properties. Of the various types of single crystal diamond that can be produced using these techniques, high quality single crystal CVD diamond can be routinely produced, and this material is playing an increasing role in research on materials under extreme conditions. This article highlights recent developments in single crystal CVD diamond synthesis and characterization, as well as various applications in high-pressure materials research.

Keywords*: single crystal diamond, chemical vapor deposition (CVD), high pressure, annealing, hardness, toughness, photoluminescence, infrared spectroscopy, cathodoluminescence, absorption, X-ray diffraction, X-ray spectroscopy, microwave, deposition, plasma.*

INTRODUCTION

Diamond is a unique material with multiple superior properties, including the highest hardness, thermal conductivity, and electron mobility, very low coefficient of friction, excellent optical, infrared and X-ray transparency, and chemical inertness. These properties make the material singularly important for scientific investigations. Of particular importance have been high-pressure experiments with diamond anvil cells (DACs). Historically, natural diamond has been used in DACs, but this material is limited in size, strength, and other physical properties in comparison to what could in principle be synthesized.

Synthetic diamond produced by high pressure-high temperature (HPHT) processes has been widely used in abrasive industry for the last 60 years [1]. Most

HPHT diamond is type I*b* with considerable amount of nitrogen incorporated during the synthesis process. This limits the broad use of such a material in a variety of applications, including scientific research using diamond anvil cells. The HPHT processes can be used to create type II*a* diamond crystals; however, the size and availability of such diamond crystals have been limited and the cost of producing such crystals remains high. Eversole [2] first reported the production of polycrystalline diamond by chemical vapor deposition (CVD) in the 1960's. Since the 1980s, advances in chemical vapor deposition technology promoted the rapid development of gas-phase synthesis of diamond. The material has been used in industrial applications such as production of abrasives, CO_2 laser windows, X-ray windows, heat spreaders, and pump seals. Although polycrystalline diamond has fulfilled some application areas, where the extraordinary physical, electrical, and electrical properties are exploited, there is still a need for large, high quality, single crystal diamond that could be used in active and passive electronic components, lasers, quantum computing, and high-pressure research.

The CVD diamond growth studies in our laboratory have been motivated in part by the need for diamond for diamond advancing for high-pressure studies of materials. In order to achieve high pressures in DACs, the diamond anvils typically must be carefully selected, cut, and polished into the appropriate shape. As per definition of pressure ($p = F/A$), an obvious way to increase the maximum pressure is to reduce area A, over which force F is acting. However, this results in a great reduction in the sample volume available for experiments. It is of interest to enhance sample volume for many high pressure studies while, at the same time, maintaining the capability of performing diverse in-situ measurements [3, 4]. This requires even larger diamond crystals.

Over the past decade, we have improved microwave plasma CVD techniques for the fabrication of high quality, large single crystal diamond at high growth rates. Yan et al. [5] reported growth rates up to 150 μm/h, i.e., up to two orders of magnitude higher than the standard processes for making polycrystalline CVD diamond at the time. The high quality and integrity of the material has been verified by Raman spectroscopy, X-ray diffraction, and photoluminescence (PL). The properties of this material can also be tuned to exhibit exceptional mechanical and superior optical properties. So far, CVD diamond single crystals over 15 carats and up to 2 cm in thickness at growth rates of about 100 μm/h have been readily produced [6, 7]. As large, perfect diamonds are neither available naturally nor by HPHT processes, such CVD single crystal diamond could lead to new classes of experiments on materials under extreme conditions, particularly at high pressures and high temperatures.

ENHANCED GROWTH BY MICROWAVE PLASMA CVD PROCESSES

Diamond growth at high gas pressure

Three major CVD diamond growth techniques employing low-pressure regime are hot-filament CVD (HFCVD), microwave plasma (MPCVD), and arc-jet torch methods. Among these three techniques, HFCVD is widely utilized to produce polycrystalline diamond films. HFCVD systems manufactured by sp^3 Company in California, USA, can provide a coating area as large as 144 square inches with ±10 % uniformity across the coated wafers. However, due to the nature of the hot filament process, the feasibility of producing diamond at high gas pressure (> 30 torr) is limited. Also, hot filament-grown materials normally serve as a contamination source and consequently deteriorate diamond quality [8, 9]. To date,

very little progress in single crystal diamond synthesis using HFCVD has been reported.

The arc-jet torch CVD method, on the other hand, can produce diamond at high growth rates. Using a modified arc-jet torch CVD system, Ohtake et al. [10, 11] demonstrated diamond growth rates exceeding 900 micron/h, with a carbon conversion efficiency of about 8 %. However, despite the high linear growth rates, the high heat fluxes and spatially limited deposits that accompanied arc-jet processes restrict projected applications to those involving direct use of the thick, free standing diamond plates. The process has not yet been sufficiently precisely controlled to obtain high-quality single crystal diamond.

MPCVD methods provide stable conditions and reproducible quality at a reasonable cost [12, 13]. In fact, steady progress in MPCVD synthesis techniques has made it possible to manufacture high quality polycrystalline CVD diamond for optical components [14, 15]. It is well known that polycrystalline CVD diamond and diamond-like carbon contain diamond grains and grain boundaries. The orientation of the diamond grains is normally random, and the grain boundary compromises the extraordinary physical properties of diamond [14, 16, 17]. The major disadvantage of traditional MPCVD methods is that only low growth rates of ~ 1 μm for polycrystalline diamond [18–21] had been reached.

Our early studies used modified 5–6 kW, 2.45 GHz ASTEX MPCVD systems. The cavity and substrate stage have been designed and optimized to sustain stable and energetic plasmas for high growth rate applications at different microwave power (1–6 kW) levels. A variety of substrates, including commercial HPHT synthetic type I*b* diamond, natural type I*b* diamond, and CVD single crystal diamond were used. The deposition surfaces were within 2–3° of the {100} crystallographic planes. The substrates had polished, smooth surfaces that were cleaned ultrasonically with acetone and mechanically mounted on a molybdenum substrate holder to ensure a uniform surface temperature. Experimental variables included the reactant gas pressure, gas chemistry, and substrate temperature.

Early studies showed that when the reactor pressure is increased from 60 to 200 torr, the diamond growth rate increased ~ 5-fold, while crystal penetration twins decreased [22, 23]. Nitrogen added to the gas chemistry also played significant role in enhancing the growth rate and promoting the formation of the {100} faces [6, 7, 15, 20]. These studies led to the first fabrication of transparent, smooth single-crystal CVD diamond. The growth morphology indicated that the <100> side-growth rate was faster than that of the <111> corner-growth rate. The value of the growth parameter $\alpha = 3^{1/2}V_{100}/V_{111}$was found to be in a range of 2.5–3.0. The optimal value for α is close to 3, which corresponds to preferential growth along the <100> direction [24, 25].

Microwave plasma hot spots formation

In order to grow homogeneous, thick single-crystal diamond, long depositions lasting many hours are required. One of the critical issues in diamond synthesis employing an MPCVD reactor is the behavior of plasma–substrate and plasma–substrate holder interactions. Figure 1 shows an example of plasma hot spots generated during synthesis of single-crystal diamond inside a CVD chamber [26]. During diamond synthesis, the growth directions and rate can vary on the diamond surface, depending on process parameters such as plasma density, substrate temperature, partial pressure, and diffusion transport. Because of a stark gradient of growth surface profile between the edge and substrate center, microwave energy couples more easily to the sharper edge, and this localized microwave coupling

onto the tip edge can cause hot spots. Moreover, the microwave energy not only breaks down the carbon-bearing molecules in the plasma, but also causes electrical breakdown and thermal instabilities via ohmic heating on the substrate tip edge. Such hot spots can have bright luminescence with measured substrate temperature over the range of 2200 °C. Typically, hot spots are observed after a diamond growth time that exceeds 24 hours, depending on the plasma density. As a consequence, the coupling of the microwave energy is mainly focused on the hot spot instead of being equally distributed across the substrate surface. Therefore, substrate surface conditions cannot be sustained, and the other materials such as graphitic or diamond-like carbon can be formed on the surface.

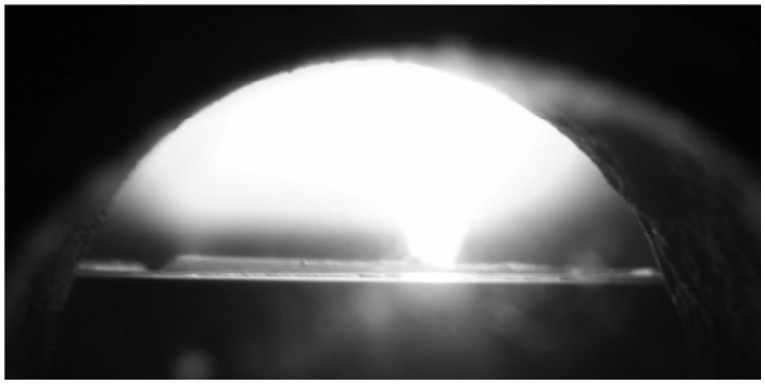

Fig. 1. Hot spot formation between plasma discharge and substrate surface tip during long growth of single-crystal diamond. The CVD reactor is a 2.45-GHz microwave cylindrical cavity reactor with TM01 mode excitation.

Optical characterization of CVD single-crystal diamond

As-grown single crystal diamond. A small addition of nitrogen to the gas synthesis can enhance growth rate, leading to diamond with a yellowish or light brown color due to broad UV-visible absorption [5, 6]. SIMS measurements of diamond grown this way showed typical nitrogen content below 10 ppm, which is comparable to that of natural type II*a* diamond, indicating that the optical absorption does not simply arise from the incorporation of nitrogen into the diamond structure. One explanation for such a coloration is the association with nitrogen–vacancy–hydrogen (NVH^-) complex centers [27]. On the other hand, addition of oxygen to the CVD diamond-growth chemistry can also facilitate the diamond formation [28]. New species formed in the plasma (i.e., O^- and OH^-) etch away impurities (hydrogen, and sp^2 carbon) and defects on growth surface more efficiently than atomic hydrogen, and therefore improve the diamond quality. Furthermore, oxygen addition can hinder diamond cracks, thereby promoting growth of thicker single crystal layers [29, 30].

As examples, two samples were produced with oxygen addition (Fig. 2). They were characterized by photoluminescence (Fig. 3) along with one natural type II*a* sample (for comparison). Nitrogen-containing single-crystal CVD diamond shows signatures of the nitrogen-vacancy centers at 575 nm (NV^0) and 637 nm (NV^-) along with a broad luminescence background. The measured natural type II*a* diamond had negligible background with the prominent feature being the first-order diamond Raman peak. The second-order Raman feature between 575 and 600 nm is also observed for the type II*a* diamond. A colorless single-crystal CVD diamond grown without nitrogen exhibits a PL spectrum similar to that of type II*a* diamond.

It is difficult to distinguish the PL spectra of the type II*a* crystal and this colorless single-crystal CVD diamond. The optical properties of these materials were further investigated by the UV-visible absorption spectroscopy (Fig. 4). The nitrogen-doped single-crystal CVD diamond exhibits typical features of brown CVD diamond, including broad bands at 270 nm (substitutional nitrogen), 370 nm, and 550 nm (nitrogen vacancy centers). There is also no significant difference in the Raman line-shape of colorless single-crystal CVD diamond and the type II*a* natural diamond.

Fig. 2. CVD single-crystal diamonds of various shapes.

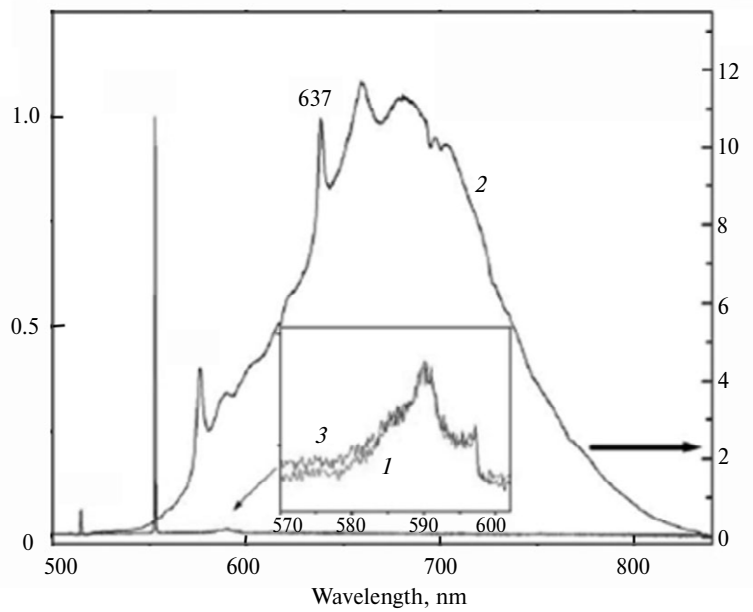

Fig. 3. Photoluminescence spectra of natural II*a* diamond (*1*), light brown (*2*), and colorless single-crystal CVD diamonds (300 K) (*3*).The intensities were normalized to the diamond first-order Raman peak. The insert shows spectra details in the 570–610 nm range (514.5 nm excitation).

Figure 5 shows the infrared (IR) absorption spectra of a light brown and colorless single-crystal CVD diamond. The broad band at 2930 cm^{-1} is attributed to hydrogenated amorphous carbon (a-C:H). In brown single-crystal CVD diamond, in the near IR region, the strong absorptions at 7358, 7234, 6857, and 6427 cm^{-1}

are attributed to hydrogen impurities from growth sector [29]. The IR spectrum of the colorless single-crystal CVD diamond is featureless in this region. The 3124 cm^{-1} peak, C–H stretching mode, is not detected either.

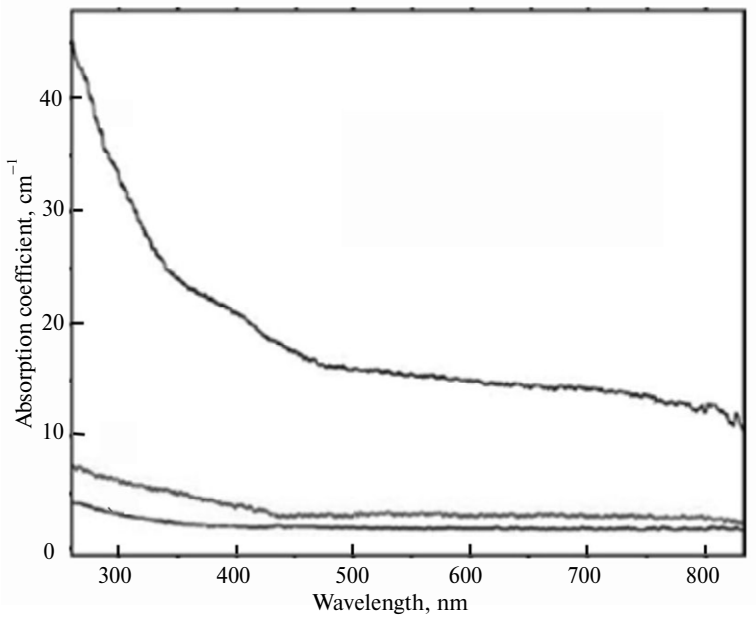

Fig. 4. UV-visible absorption spectra of nitrogen-doped (*1*) and colorless (*2*) single crystal CVD diamond, and natural type II*a* diamond (*3*).

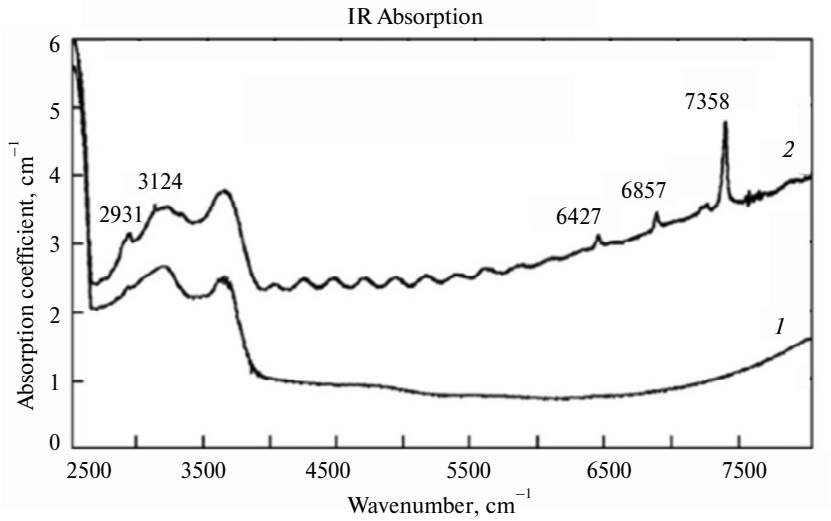

Fig. 5. Infrared absorption spectra of near colorless (*1*) and light brown (*2*) single crystal CVD diamond.

Large, transparent single crystals. As mentioned above, with the nitrogen addition to the synthesis gas, fabrication of single crystal CVD diamond at high growth rate can lead to diamond with a yellowish or light brown color. This type of diamond is suitable for many high-pressure experiments such as X-ray diffraction. Such diamond is also useful for applications like cutting and abrasion. However,

many optical applications regimes call for highly transparent, fluorescence-free diamond.

The 2.3-carat anvil shown in Fig. 6 provides a useful example of the current state of the art. The as-grown CVD diamond is measured 8.5×8.5×2 mm, and it only contains very few inclusions on the girdle. There was no evidence for layers caused by multiple growths and striations associated with differential uptake of defects on the risers and terraces of growth steps (as observed in [31]). Figure 7 shows transmittance spectra, measured at 300 K, of representative CVD samples. Sharp diamond first-order and second-order Raman features were measured (Fig. 8) and no PL peaks at 575 nm and 637 nm caused by NV^0 and NV^- centers were evident. The intensity ratio of the second-order Raman peak to the fluorescence background exceeded 5, a measure of high optical quality. Cathodoluminescence (CL) of the nitrogen-containing CVD diamond typically displays strong orange emission. In addition, the absorption at 737 nm from the siliconvacancyrelated (SiV) center is invisible or very weak. It is clear that the material grown here is largely free of this emission (see Fig. 8).

Fig. 6. The picture at right shows a 2.3-carat single-crystal CVD diamond compared with a 0.25-carat CVD diamond. Inserts (*a*–*d*) demonstrate the evolution of CVD diamond single crystal starting with as-grown 13.5-carat block (*a*) to the 2.3-carat cut gem anvil (*d*).

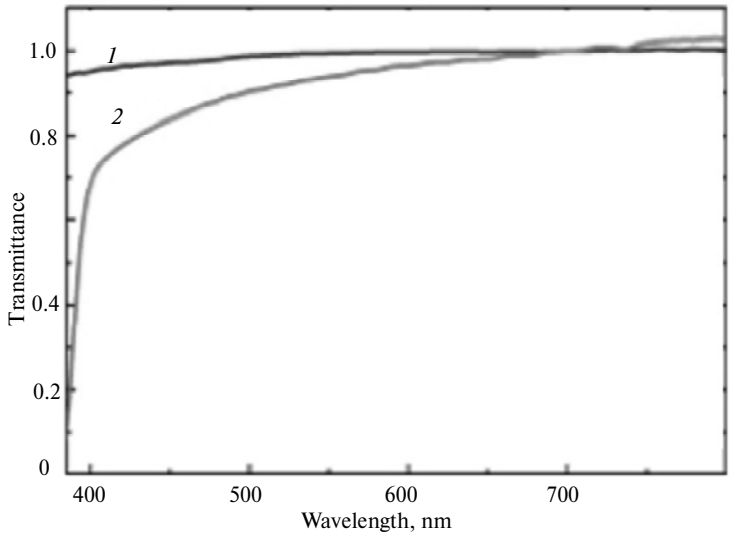

Fig. 7. UV-visible transmission spectra of the 0.5 (*1*) and 5 mm (*2*) thick CVD diamond plates.

Confocal Raman/PL measurements at room temperature were used to examine possible inclusions in this crystal. Figure 9 shows the Raman imaging results for a

small (around 30 μm) black inclusion close to the girdle. The first-order Raman peak, the broad G band of amorphous carbon, the 1610 cm^{-1} caused by graphite and nanocrystalline diamond were uncovered. The peak at 1120 cm^{-1} indicates of carbon–hydrogen bonds in grain boundaries, together with the presence of the D band at 1350 cm^{-1} and G band at 1560 cm^{-1}, indicate the existence of polycrystalline diamond perhaps at the nanosize. Residual nitrogen within the MPCVD system and the reaction gas sources (CH_4, H_2) are largely responsible for the unintentional heterogeneity within the crystal, as observed above. SiO_2 windows of the reaction chamber, on the other hand, are accounted for the incorporation of silicon impurity in the material.

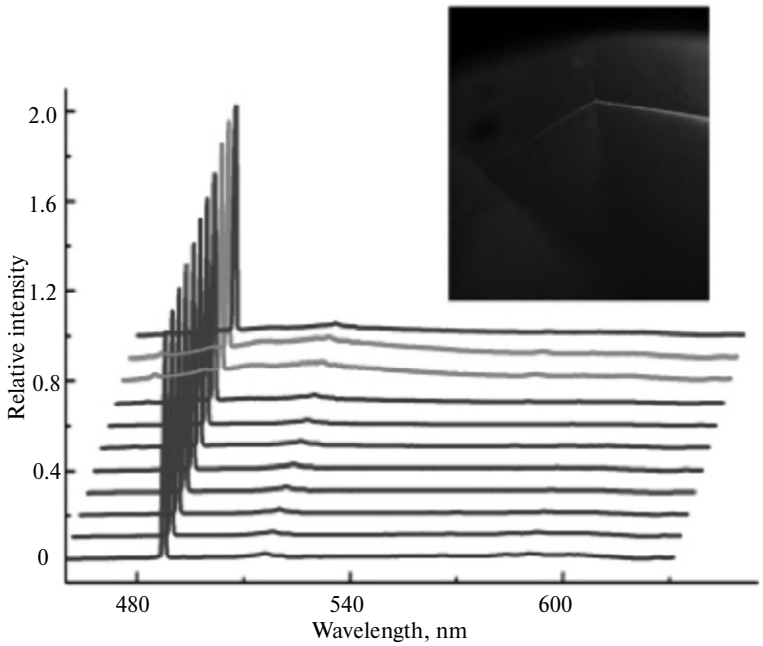

Fig. 8. Photoluminescence (PL) and Raman spectra measured along the growth direction from culet to girdle of the 2.3-carat anvil.

POST-GROWTH TREATMENTS

Optical enhancement by HPHT

HPHT annealing. HPHT annealing processes are frequently used to improve the optical properties of natural diamonds [32–36]. An example of this process is the so-called GE-POL or Bellatarie process, where nitrogen-free brown diamond is converted into a colorless diamond [32]. Other color changes can also be performed: the color of brown nitrogen-containing diamond can be changed into a yellow-green [33] or vivid yellow color.

The HPHT treatment processes have been successfully applied to nitrogen-containing CVD single crystal diamond. Detailed optical analyse, including PL, UV visible absorption, IR absorption and CL topography has been reported [37]. In general, annealing at high pressures and temperatures can significantly alter the material. The majority of nitrogen in the investigated samples was in the form of isolated nitrogen at a carbon substitutional site and remained this way throughout the HPHT annealing. In as-grown sample, nitrogen-vacancy related centers NV, NV^-, and NVH^- were observed and they either disappeared or transformed into

more complex centers (H3 and N3), believed to be N–V–N and N–N–N–V, respectively, upon annealing. The HPHT treatment at relatively low temperatures shows evidence of NV center dissociation and vacancy diffusion, but little evidence of N diffusion in the lattice, while the higher temperature treatments suggest the mobility of N to form N–N related centers. Tightly bound hydrogen to carbon is evident in the as-grown and annealed samples, indicating that it remains in the lattice throughout the annealing process, while the vibrational frequencies (modes) do shift and change as a result of annealing. Many new and unassigned spectral features were observed in the spectra of the samples.

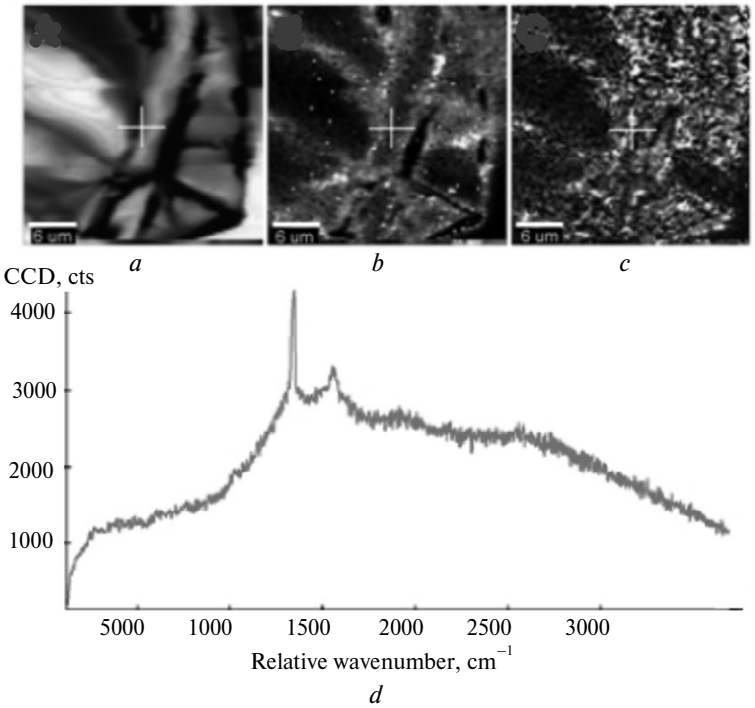

Fig. 9. Confocal Raman mapping of an inclusion in the CVD diamond, (*a*) map of diamond peak intensity, (*b*) map of the broad G band caused by amorphous carbon, (*c*) map of 1610 cm^{-1} peak caused by graphite or nanocrystalline diamond, (*d*) Raman spectrum of the inclusion showing the bands at 1332 and 1610 cm^{-1}.

LPHT annealing. Another effective way to enhance the optical properties of CVD diamond is annealing conducted inside the CVD reactor at high temperature but very low pressure (less than 300 Torr). Diamond of course unstable at atmospheric pressure and all temperatures [13]. To prevent graphitization, high temperatures (e.g., ~1600 °C) and high pressure annealing is typically needed [13]. Studies of the effects of the single-crystal CVD diamond exposure to high temperatures (up to 2200 °C) and low (i.e., below atmospheric) pressure reveals significant changes in the optical properties of diamond without of significant graphitization. Reduced oxygen and high hydrogen concentration in the gas appeared to be key factors.

Single-crystal CVD diamond plates produced with nitrogen concentrations around 10 ppm and thicknesses of 0.2–6.0 mm were subjected to low pressure–high temperature (LPHT) processing at temperatures of 1400–2200 °C and pressures lower than 300 torr. Figure 10 shows some examples of transparent single-crystal CVD diamond plates after the treatment. The LPHT- treated samples were subsequently characterized by PL, IR, and UV-Visible absorption measurements.

A detailed analysis of PL and IR can be found in our previous publication [27]. Changes produced by LPHT treatments are reflected in the large decrease in UV-visible absorption. The absorption coefficients were lower after the annealing process by factors 2 to 6 and similar to those determined after HPHT annealing [31, 37]. No significant change in the UV-visible absorption of this type CVD diamond was observed after annealing at temperatures lower than 1600 °C.

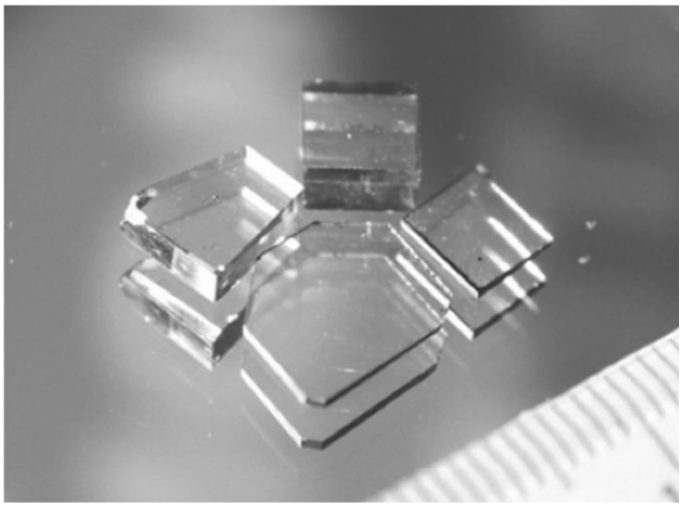

Fig. 10. Transparent LPHT-treated (up to 2000 °C) single-crystal CVD diamond plates produced at high growth rates.

The LPHT annealing effects are broadly similar to those of HPHT annealing, but with the following differences: the LPHT-annealed and as-grown CVD diamond both exhibit a peak at 3124 cm^{-1} and bands at 7357, 7220, 6856, and 6429 cm^{-1} that are not observed in the HPHT-treated CVD diamond. The LPHT-treated CVD diamond does not exhibit the 3107 cm^{-1} absorption feature [38], related to gray color and existing in the HPHT annealed samples, and the bands at 2972 and 2991 cm^{-1}. Finally, the high-pressure-induced sp^3 C–H bond shift by 3–15 cm^{-1} to higher wave numbers at 2820, 2873, and 2905 cm^{-1} that is present in the HPHT-annealed samples is absent in the LPHT-treated crystals.

A comparison of UV-visible, PL and IR measurements on LPHT-treated CVD diamond crystals with data on diamond subjected to HPHT annealing yields insights into the origin of the diverse spectroscopic features. Hydrogen is usually the most abundant impurity in the diamond grown during CVD synthesis. It is suggested that hydrogen migrates above 1400 °C. The formation of brown diamond could be due to the enhancement of growth rate by nitrogen present in the gas used for the CVD growth; diamond produced at this high growth rate has more extended defects such as under-bonded carbon or vacancy clusters. Nitrogen can decorate these defects and hydrogen is incorporated with those defects forming unstable centers: a-C:H (and other hydrogen-related infrared absorption bands) and NVH^- [39]. Both HPHT and LPHT annealing mobilize the incorporated hydrogen. There is evidence [40, 41] that the annealing of a polycrystalline CVD diamond at 1400 °C causes hydrogen located on internal grain boundaries or in the intergranular material to become mobile. IR absorption spectra, after annealing, reveal that the concentration of a-C:H decreases and hydrogen forms stable C–H bonds on the {100} and {111} planes.

Hardness and toughness enhancements

A common technique to evaluate the hardness and fracture toughness of numerous materials is to use the Vickers microhardness testing [40–42]. Using this approach we have demonstrated that the high-growth rate single-crystal CVD diamond has extremely high hardness [43]. Here we summarize some of the extraordinary mechanical properties of this type of CVD single crystal diamond.

Detailed description of experimental setup can be found in previous publications [43–45]. To prevent elastic deformation of the indenter and to eliminate surface effects, relatively high loads of 1 to 3 kg were utilized on smoothly polished {100} faces in the <100> direction of the diamond. A comparison study was done on various types of natural diamonds (I*a*, II*a*, and I*b*) to validate our results. Our measured fracture toughness values for I*a* and II*a* are 8.5 (±2.5) MPa·$m^{1/2}$ and 5.2 (±2.2) MPa·$m^{1/2}$, respectively, in good agreement with published data [46, 47].

Figure 11 shows the indentation patterns of various diamond crystals. For CVD diamond, all indentations exhibit square crack patterns along the softer <110> and <111> directions and no cross-like crack line along the <100> direction, and show deformation marks produced by the pyramidal indenter. The indentation measurements reveal that the annealed CVD diamond is ultrahard (at least ~ 160 GPa), beyond hardness of annealed or unannealed type I*b* (~ 90 GPa), I*a* (~ 100 GPa), and comparable to the most perfect annealed II*a* (~ 140 GPa) diamond. Annealed dark brown diamond grown with high nitrogen (~ 4 % N_2:CH_4) and at high temperatures (> 1300 ºC) possesses square fracture patterns; however, after annealing the darker CVD crystal cannot be readily indented. Circular indentation patterns seen after annealing in the colorless diamond grown at low N_2:CH_4 ratio (~ 0.4 % N_2:CH_4) and about 1200 °C are similar to those of annealed natural type II*a* diamonds.

We also performed hardness and toughness measurements for diamond doped with boron. These boron-containing single crystals were also synthesized by high-density MPCVD using the similar growth parameters as described above. Hardness–fracture toughness data are plotted in Fig. 12 for natural I*a*, II*a*, synthetic I*b*, single-crystal CVD, and boron-doped single-crystal CVD diamonds. Without boron doping, single-crystal CVD diamond grown by H_2/CH_4/N_2 chemistry has a fracture toughness of 15.2 (±4.8) MPa $m^{1/2}$, as compared to 8 (±4) MPa $m^{1/2}$ for natural I*a*, II*a*, and colorless CVD single-crystal diamond grown without the addition of N_2 to the feed gas, and 10 (±2) MPa $m^{1/2}$ for I*b* synthetic yellow diamond. Measured fracture toughness of boron- doped single crystal CVD diamond is between 22 and 34 MPa $m^{1/2}$. It is clear that boron doping of single-crystal CVD diamond can significantly improve the fracture toughness by at least a factor of two, without compromising the hardness [78 (±12) GPa].

It may be argued that quantitative measurements on materials having fracture toughness higher than 30 MPa $m^{1/2}$ exceed the limit of Vickers techniques. However, it is important to note that the behavior of the diamond material studied here is qualitatively different. Specifically, there is lack of a visible trace of cracking along the indentation craters (see Fig. 11). All indentation patterns on the boron-doped single crystal CVD diamond exhibit square crack patterns along the softer <110> and <111> directions, but the material is free of crack lines along the <100>. Unlike indentation craters on natural or type I*b* diamond crystals, which typically contain cross-like cracks along all of the above directions, the fracture pattern on these crystals is more predictable and can be engineered to further improve fracture resistance in mechanical and abrasive applications.

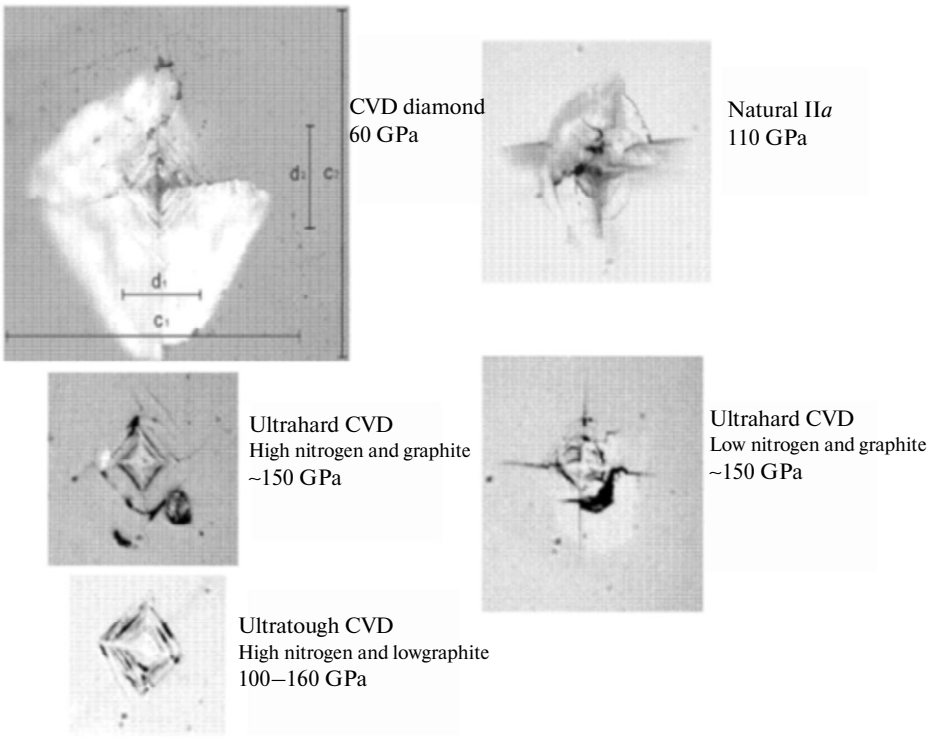

Fig. 11. Indentation patterns for as-grown CVD single-crystal diamond, natural II*a* diamond, HPHT-annealed CVD single-crystal diamond, and annealed ultratough CVD single-crystal diamond.

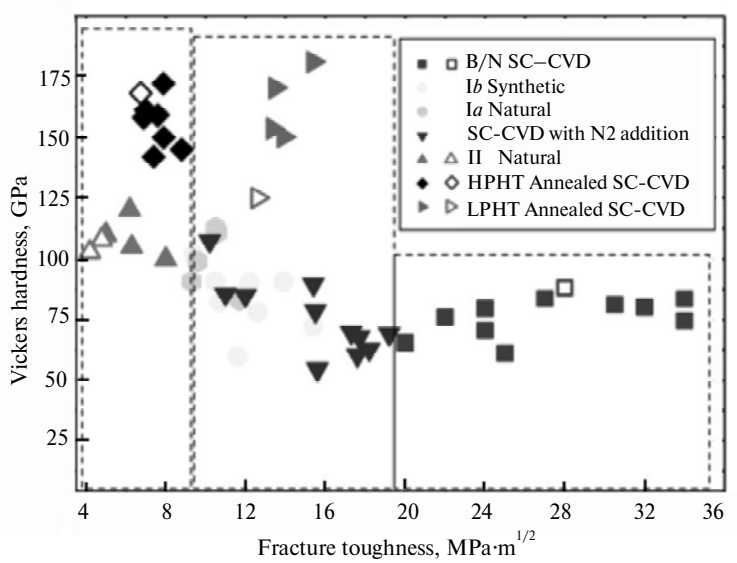

Fig. 12. Vickers hardness and fracture toughness on {100} faces of various diamonds in the <100> direction. Three zones are defined: the reported and measured values for natural type I*a* and II*a* diamond are on the left; the center zone includes type I*b* and CVD diamond; the right zone includes boron-doped CVD diamond.

It has been reported that incorporation of nitrogen in the growth chemistry significantly enhances the formation of the {100} growth facets, as nitrogen atoms

preferably incorporate into the {100} growth surface [5, 48]. However, boron species greatly enhance the formation of octahedral growth facets and preferably incorporate into the {111} growth surfaces [49]. Therefore, the enlargement of the boron-doped CVD diamond layer is not applicable due to the discontinuity in the octahedral structure [50]. Diamond substrates in our studies were oriented to within 3° of the {100} plane (the uncertainty in the laser sawing technique). The co-doping mechanism can be described by the step-flow growth process [51]. In this process, nitrogen atoms appear to enhance the formation of the microterraces, while boron atoms can be doped between individual steps. Therefore, a continuous step-flow growth surface is formed for further CVD layer enlargement.

Unlike diamond treated for surface toughening by ion-implantation [52] or surface thermal diffusion [53], all CVD diamond crystals in this study were extensively polished prior to the indentation. The results therefore demonstrate that the toughness enhancement is a bulk property. The IR and PL spectra indicate that boron and nitrogen (NV^0 center at 575 nm) atoms coexist in the diamond structure [45]. It is possible that the interaction among nitrogen, boron, and adjacent carbon atoms can lead to the highly improved toughness. More detailed understanding of the mechanism of the toughness enhancement by the boron–nitrogen co-doping will require additional experiments and modeling. Figure 12 shows that all boron-doped CVD diamonds have slightly higher hardness as compared to undoped CVD diamond. The enhanced growth of both the {100} and {111} growth sectors appears to strengthen the diamond considerably, as predicted in [54].

X-ray topography

We have shown that CVD diamond can be grown in such a way that it exhibits hardness very comparable to the hardness of natural diamond but larger toughness. To understand the origin of the enhanced toughness, we used the 3D microdiffraction techniques, which allow measurements of local lattice rotations and residual strains with a 1 μm resolution. We utilized the beamline 34IDE at the Advanced Photon Source (APS), Argonne National Laboratory (ANL). Differential aperture X-ray microscopy reveals [55] the depth resolution of 1 μm along the X-ray beam pass. The typical incident beam size was about 0.5×0.7 μm^2. By scanning a knife-edge wire above the sample and taking the difference of adjacent white beam Laue diffraction patterns, one can sort the diffraction information from each depth along the incident beam pass at the micron resolution. A schematic of the experimental setup is shown in Fig. 13 (an area of 50×8 μm^2 was measured). The reconstructed Laue patterns were then analyzed to obtain the local lattice orientation and strain tensors. The total angular range of local crystal orientations was within 0.06 degrees. The three major components (ε_{xx}, ε_{yy}, ε_{zz}) of the strain tensor at each measured location were then calculated. The strain levels were within $\pm 2 \cdot 10^{-3}$. We concluded that the strain in the x-direction (measured by ε_{xx}) was mostly negative, while in the y-direction (measured by ε_{yy}) was mostly positive, and the crystal was nearly strain-free, as measured by ε_{zz}. Two high-strain bands existed in both ε_{xx} and ε_{yy} maps, which indicated extended regions of large local strain. The inhomogeneity of the strain distribution indicates the local defect arrangement.

The geometrically necessary dislocation (GND) density was used to describe the orientation gradient. Considering total 36 slip systems in face-centered-cubic structure, we found that the <110>{111}-type dislocations were dominant. Combinations of these 36 slip systems to accommodate the lattice rotation and minimize the total GND density were analyzed. A simplex method was utilized to achieve the GND density for the area measured. The density was calculated based on the

orientation change in 2d plane only. The real density is expected to be higher than these values due to the lack of orientation gradient in the third direction. The GND density map revealed that the highest GND density was $1.7 \cdot 10^8$ cm^{-2}, while the overall density was about $4 \cdot 10^7$ cm^{-2}.

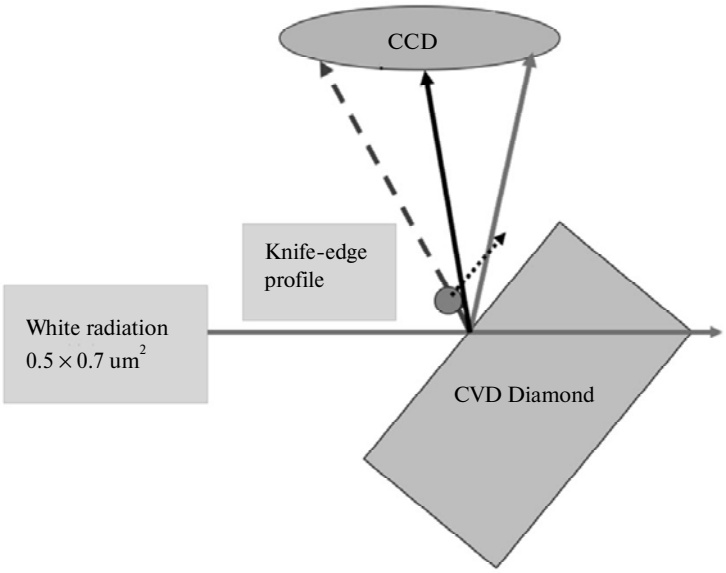

Fig. 13. Schematic layout of X-ray high-resolution measurement.

Preliminary evaluations of a series of as-grown CVD diamond single crystals using the white beam topography technique were also performed. The experiments were conducted at the APS beam line 16BM-B. These crystals were positioned in the beam with the growth axes parallel and/or normal to the beam direction and irradiated with the full spectrum of synchrotron radiation. Multiple X-ray topograms corresponding to reflections from different crystallographic crystal planes were recorded on an X-ray film placed behind the sample at a distance of about 20 cm. Due to the high collimation of the synchrotron radiation, high-resolution images of defects present in the crystal could be produced. A typical example of the images obtained is shown in Fig. 14.

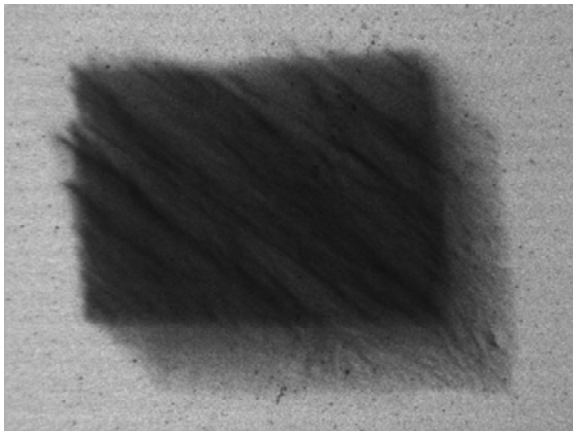

Fig. 14. Example of an X-ray topograph, corresponding to a single reflection from a CVD single crystal, using synchrotron-radiation white-beam topography.

APPLICATIONS IN EXTREME CONDITIONS SCIENCE

Ultrahigh pressure experiments

Diamond anvil cell (DAC) techniques have become powerful and versatile tools for a wide range of high-pressure measurements [3, 56–58]. DAC devices typically use natural single crystal diamonds, though high-purity HPHT diamond is also being used increasingly for some experiments [59, 60]. Some unavoidable anvil damages typically occurs when experiments are conducted above one megabar. Some measurements require large sample volumes (e.g., in neutron diffraction and NMR measurements), and the available sizes of high quality natural diamonds are restricted. Single crystals of moissanite and sapphire have been introduced and used as anvil material [61, 62], but their lower strength limits the pressure range possible to reach with such anvils.

Understanding the behavior of gas mixtures samples at high pressure is an important research field in physics, chemistry, and planetary sciences. Using inert gas as the pressure medium in the pressure chamber of the diamond anvil cell is a key technique for producing nearly hydrostatic pressure conditions. Natural diamond anvils tend to fail, particularly at high temperature when they confine dense gases at high pressures; this has been ascribed to defects that can be invisible at the culet surfaces [63, 64]. Hydrogen and helium are the most difficult samples in simultaneous high p, T environments. Thus, efforts for developing new types of anvils for high p, T devices are useful for studying these fundamental systems at extreme conditions [57, 65, 66].

During high pressure experiments, it was observed that the damage to the diamond anvil frequently occurred near or around the very tip. One approach to using single-crystal CVD diamond in high-pressure research is to remove the top damaged part of a damaged anvil by sawing and to grow a CVD diamond layer on the top of remaining part of the anvil. We performed such “repairs” of damaged anvils and made them usable for further experiments. Figures 15 and 16 present the schematic of the repair method and a picture of an anvil after CVD layer deposition. The tip of the diamond grows into a square block where four sides can be determined as the {100} planes. After reshaping/polishing, a modified double-bevel anvil with the final culet diameter of 30 μm was obtained. The thickness of the CVD layers on the top of polished anvils ranged from 0.3 to 0.5 mm.

Hydrogen and helium confinement at high p, T conditions is one of the most stringent test of diamond anvils [67]. Measurements on hydrogen at simultaneous high pressure and temperatures were performed using various anvils that had been augmented by CVD processes. A pair of CVD-covered diamond anvils was polished to double-beveled shape with the diameters of the central flats (culets) between 30 and 40 μm. Tungsten was chosen as the gasket material and indented by the anvils inside a DAC to a thickness of 10 μm. A small (20 μm in diameter) hole was drilled in the center of the indentation. High-purity hydrogen gas was then loaded using a pressure gas-loading apparatus [68]. External heaters were mounted surrounding the upper and lower diamonds. A K-type thermocouple was placed in contact to one of the diamond tips for a temperature measurement. Pressure at room temperature was determined by hydrogen vibron positions, which were calibrated previously against the ruby pressure scale [63, 67]. Quasi-isobaric data collection was used at different temperatures. Pressure could change 5–15 % during the heating, and it was monitored from the Raman signal of the anvils [69–71].

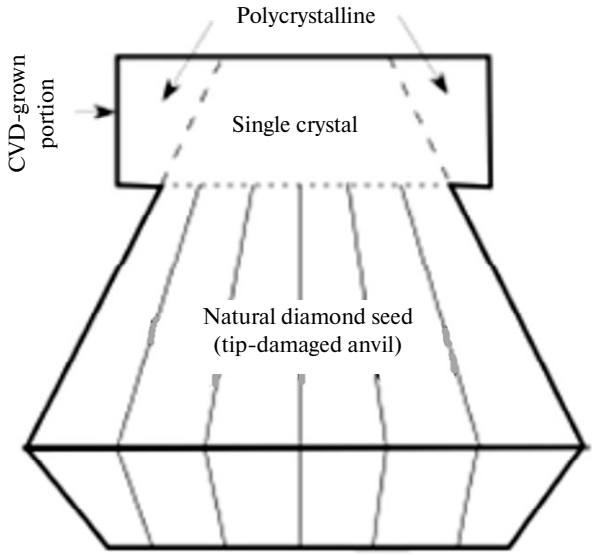

Fig. 15. Scheme of a repair method of an anvil: damaged culet is replaced by a CVD layer.

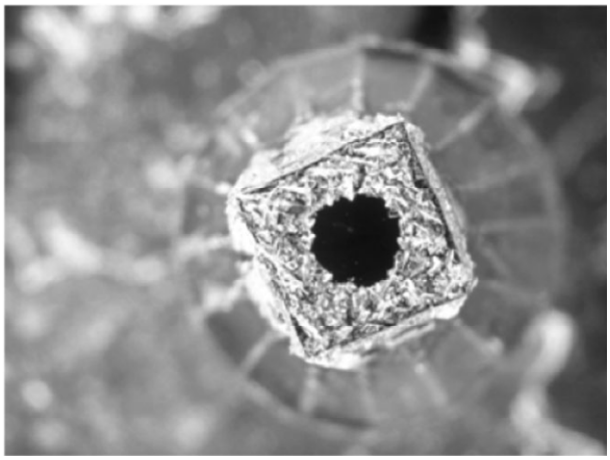

Fig. 16. Natural diamond anvil with an as-grown single-crystal layer of CVD diamond.

Figure 17 shows the high and low frequency Raman modes of hydrogen measured during the external heating at a starting pressure of 114 GPa at room temperature [71]. The vibron shows strong softening with temperature consistent with previous studies [67]. The low-frequency modes at high temperatures were also observed. This experiment was terminated by the heater failure rather than by the failure of the anvils. The sample and diamonds survived these *p, T* conditions in contact with hydrogen; the anvils were damaged during the pressure release.

Small angle X-ray scattering

Small angle X-ray scattering (SAXS) is a powerful method for analyzing the structure of materials. High quality type II*a* single-crystal diamond has been found to be an ideal candidate for the X-ray windows of the sample cell. Here we demonstrate the performance of high optical quality CVD single crystal diamond with low nitrogen content under synchrotron SAXS studies.

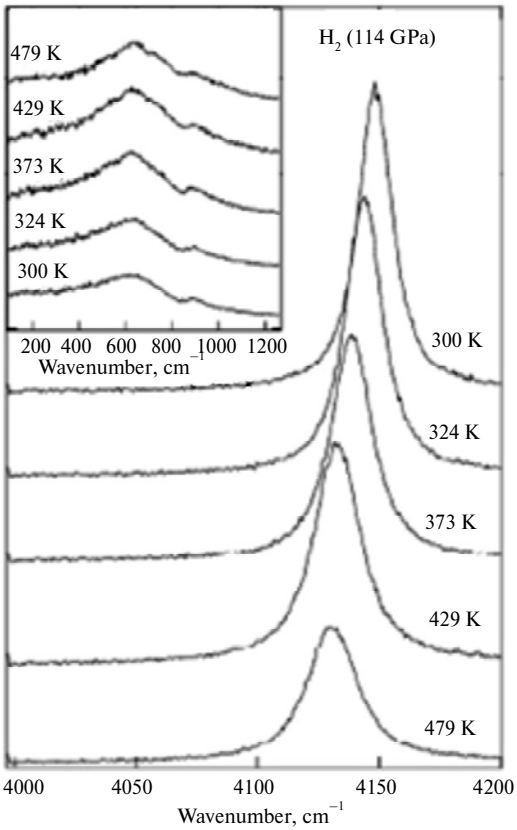

Fig. 17. High and low frequency Raman modes of hydrogen measured with the use of a pair of composite anvils during the external heating starting with 114 GPa pressure and room temperature .

Selected samples of near colorless and colorless single crystal CVD diamonds were used in this study (Fig. 18, *a*) [72]. Synchrotron SAXS measurements were performed at the CHESS G1 Station, where X-ray beams had fluxes of 10^{10}–10^{12} photons/s at energies of 9.5 to 12 keV. Figure 18, *b* shows the SAXS beamline setup. In order to prepare SAXS experiments, additional X-ray topography checks of the windows were done at the CHESS A2 station. For large diamonds (> 2.5 mm), camera was translated horizontally and vertically to obtain the overall topography. Because all the diamond windows were cut in such a way that the <001> direction was roughly along the surface normal, the reflection geometry was used to record the {004} projection topography images.

SAXS scattering from an ideal window (or system parasitic scattering) should be less than the scattering from the sample being studied. This requirement is particularly stringent in protein solution experiments, where a weak scattering from dilute protein solutions must be accurately measured. In a typical SAXS beamline such as CHESS G1 station (see Fig. 18, *b*), vacuum or helium-flushed flight path was installed to minimize the background (air scattering). The three windows in the flight path that the X-ray beam passes through sequentially were two 12 μm thick Kapton and one 50 μm thick mylar films, which can hold reasonably high vacuum (~ 5 mTorr) and produce very low background scattering. Thin Kapton films yield very little scattering and are typically used in protein solution SAXS [73]. However, an undoped 500 μm thick single-crystal CVD diamond grown in the atmosphere without intentional nitrogen addition had comparable SAXS signal to the background scattering of the direct beam, and showed even smaller or comparable scattering than a single 7.5 μm thick Kapton film, demonstrating that undoped single-crystal CVD diamond is an excellent window material for SAXS [72]. Comparison studies with a type I*a* natural diamonds display more intense and/or anisotropic scattering as previously observed [74, 75]. In one case, intense and isotropic scattering was observed (Fig. 19, *b*). The undoped single-crystal CVD diamond crystals presented here (see Fig. 19, *a*) show no anisotropy in the scattering and are thus very promising material for SAXS windows, in particular for macromolecules such as proteins.

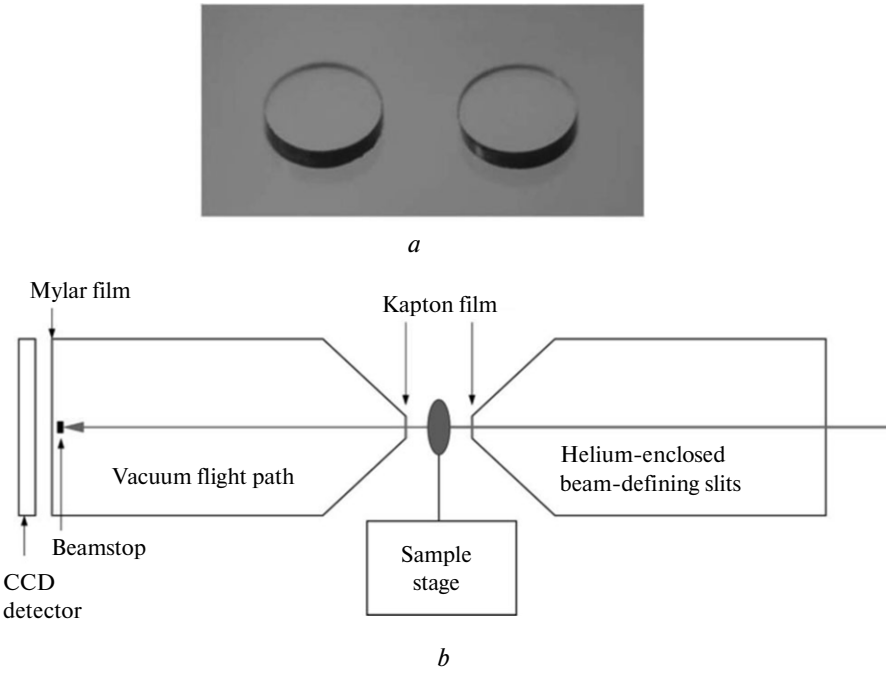

a *b*

Fig. 18. (*a*) Single-crystal CVD diamond windows for SAXS: 3.0 mm in diameter and 0.5 mm in thickness; (*b*) a simplified diagram of the SAXS beamline layout. The three windows along the X-ray beam path are two 12 μm thick Kapton and one 50 μm thick mylar films.

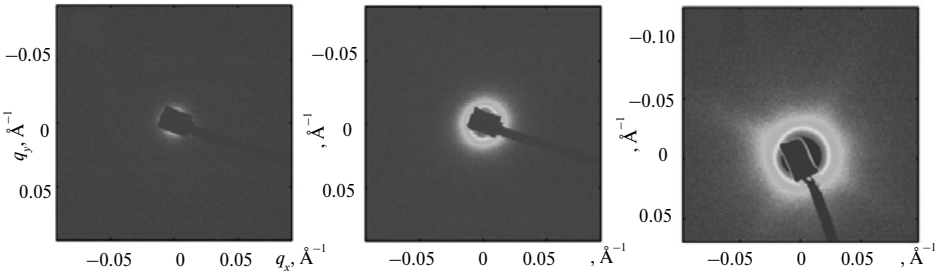

a *b* *c*

Fig. 19. (*a*) SAXS image of an undoped single-crystal CVD diamond, (*b*) a SAXS image of a type I*a* natural diamond displaying strong but isotropic scattering, and (*c*) a SAXS image of another natural diamond displaying strongly anisotropic cross-shaped scattering.

Scanning SAXS experiments were performed on several single-crystal CVD diamond crystals. The results indicated that undoped single-crystal CVD diamond has shown uniform and less scattering across different regions while nitrogen-rich single-crystal CVD diamonds had more variations in scattering at different locations. The X-ray topography was performed on both single-crystal CVD diamond and natural diamond in order to understand the origin of strong SAXS. As shown in Fig. 20, natural diamond exhibits very different topography from single-crystal CVD diamond. Line defects such as dislocations and planar defects/stacking faults can be observed in natural diamond (see Figs. 20, *a* and *b*), while dislocations are dominant in single-crystal CVD diamond (see Figs. 20, c and *d*). These dislocations have line directions close to the <001> growth direction of single-crystal CVD diamond as previously observed [76]. In several CVD diamond single crystals, viewing only part or one section of the diamond, when rocking crystal near the

diffraction angle, suggests that diamond lattice planes are bent, an effect that originates from specific growth parameters used [77]. However, this bending is not responsible for strong SAXS scattering since single-crystal CVD diamond producing no or strong parasitic scattering may both have bent planes (see Figs. 20, *e* and *f*).

A comparison of the scanning SAXS and topography data shows that nitrogen-rich regions with variable scattering correlate. In addition, undoped single-crystal CVD diamond (see Fig. 20, *d*) showing negligible scattering also contain many line defects (dislocations). The results suggest that the line defects revealed by topography do not cause strong scattering at typical q ranges for SAXS. The correlation between scattering and photoluminescence data suggests that the increased incorporation of smaller scale defect clusters (vacancy clusters, and clusters composed of nitrogen and vacancy) is the cause of the strong SAXS signal in these CVD diamond single crystals, which is associated with higher growth rates catalyzed by the presence of nitrogen.

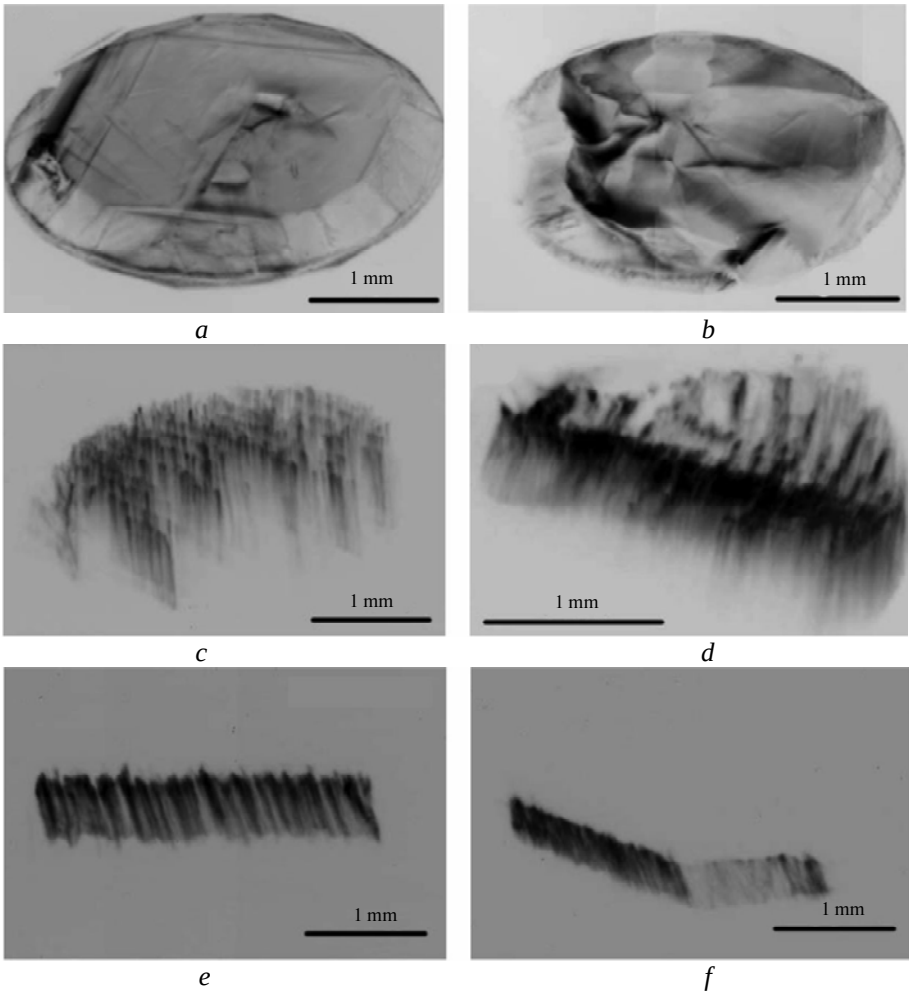

Fig. 20. {004} projection topography images of natural and single-crystal CVD diamond: (*a*) a natural diamond that displays little parasitic scattering; (*b*) the type I*a* natural diamond displaying strong scattering. (*c*–*f*) Undoped single-crystal CVD diamond.

The performance of single-crystal CVD diamond as window materials for protein solution SAXS was examined in a high-pressure protein unfolding study. An undoped single-crystal CVD diamond window (see Figs. 19, *a* and 20 *d*) was used to replace a strongly scattering natural diamond (see Fig. 19, *c*) in a previously reported high-pressure SAXS cell [73]. The destabilized AL99 mutant of T4 lysozyme was characterized by up to 300 MPa [78]. No pressure dependence was observed for the window scattering, enabling unambiguous background subtraction and subsequent Guinier analysis [72]. The results demonstrate that high quality single-crystal CVD diamonds synthesized by MPCVD methods is an excellent window material for protein solution SAXS studies, while displaying superior mechanical properties as compared to typical window materials [72, 78].

SUMMARY

Interest in the use of single crystal diamond in a variety of applications has grown as a result of the advances in microwave plasma CVD technology, leading to the fabrication of large single crystal diamond exhibiting a variety of tunable properties. The quality of single-crystal CVD diamond has improved dramatically by changes in both growth technique and post growth enhancements. Further improvements in CVD technology will enable more applications. In particular, further refinements in the growth of large, ultrahard-ultratough single-crystal CVD diamond will open the door to new studies of materials under extreme conditions.

The authors thank C. S. Zha, Y. Meng, Z. Liu, A. Steele for their help and input in preparation of this review.

This work was supported by NSF, DOE/NNSA, and WDLP.

За останні кілька роки синтез монокристалів алмазу мікрохвильовим плазмовим хімічним осадженням з газової фази з високою швидкістю значно просунувся. Прогрес було досягнуто у рості, оптичних і механічних властивостях. З різних типів монокристалічного алмазу, що можна отримати з використанням цього методу, регулярно виробляють високоякісні монокристалічні CVD-алмази, і цей матеріал відіграє все більш важливу роль при дослідженні матеріалів в екстремальних умовах. У даній роботі висвітлено останні досягнення в синтезі монокристалічного CVD-алмазу і дослідженні його характеристик, а також його різне застосування у дослідженні матеріалів при високому тиску.

***Ключові слова**: монокристалічний алмаз, хімічне осадження з газової фази (CVD), високий тиск, відпал, твердість, в'язкість, фотолюмінісценція, інфрачервона спектроскопія, катодолюмінесценція, поглинання, рентгенівська дифракція, рентгенівська спектроскопія, мікрохвильовий, осадження, плазма.*

За последние несколько лет синтез монокристаллов алмаза микроволновым плазменным химическим осаждением из газовой фазы с высокой скоростью значительно продвинулся. Прогресс был достигнут в росте, оптических и механических свойствах. Из различных типов монокристаллического алмаза, которые могут быть получены с использованием этого метода, регулярно производят высококачественные монокристаллы CVD-алмаза, и этот материал играет все более важную роль в исследовании материалов в экстремальных условиях. В этой работе осветлены последние разработки в синтезе монокристаллов CVD-алмаза и исследовании его характеристик, а также его различное применение в исследовании материалов при высоком давлении.

***Ключевые слова**: монокристаллический алмаз, химическое осаждение из газовой фазы (CVD), высокое давление, отжиг, твердость, вязкость, фотолюминесценция, инфракрасная спектроскопия, катодолюминесценция, поглощение, рентгеновская дифракция, рентгеновская спектроскопия, микроволновый, осаждение, плазма.*

1. *Hall H. T.* The synthesis of diamond // J. Chem. Educ. – 1961. – **38**, N 10. – P. 484–488.
2. *Pat. 3030188 US, IPC: B01J3/06.* Synthesis of diamond / W. G. Eversole. – Publ. 17.04.62.

3. *Jayaraman A.* Diamond anvil cell and high pressure physical investigations // Rev. Modern Phys. – 1983. – **55**. – P. 65–108.
4. *Hemley R. J., Percy W.* Bridgman's second century // High Press. Res. – 2010. – **30**, N 4. – P. 581–619.
5. *Yan C. S., Vohra Y. K., Mao H. K., Hemley R. J.* Very high growth rate chemical vapor deposition of single crystal diamond // Proc. Nat. Acad. Sci. – 2002. – **99**, N 20. – P. 12523–12525.
6. *Ho S. S., Yan C. S., Liu Z. et al.* Prospects for large single crystal CVD diamonds // Indust. Diamond Rev. – 2006. – **66**, N 10. – P. 28–32.
7. *Liang Q., Chin C. Y., Lai J. et al.* Enhanced growth of high quality single crystal diamond by MPCVD at high gas pressures //Appl. Phys. Lett. – 2009. – **94**, art. 024103.
8. *Chifre J., Lopez F., Morenza J. L., Esteve J.* Analysis of contamination in diamond films by secondary ion mass spectroscopy // Diamond Relat. Mater. – 1992. – **1**. – P. 500–503.
9. *Gheeraert E., Deneuville A., Brunel M., Oberlin J. C.* Tungsten incorporation in diamond thin films prepared by the hot-filament technique // Ibid. – **4**, N 5–6. – P. 504–507.
10. *Ohtake N., Yoshikawa M.* Diamond film preparation by arc discharge plasma jet chemical vapor deposition in the methane atmosphere // J. Electrochem. Soc. – 1990. – **137**, N 2. – P. 717–722.
11. *Ohtake N., Kuriyama Ya, Yoshikawa M. et al.* Development of an arc-discharge plasma apparatus for the high-rate synthesis of diamond // Int. J. Japan Soc. Prec. Eng. – 1991. – **25**, N 1. – P. 5–10.
12. *Characterization* of Plasma Process / Eds. P. K. Bachmann, H. Lydtin // Materials Research Society Symposium Proceedings, Warrendale, 1990.
13. *Field J.* The Properties of natural and synthetic diamond. – London: Academic, 1992.
14. *Sussmann R. S.* Diafilm, a new diamond material for optics and electronics // Indust. Diamond Rev. – 1993. – **53**. – P. 63–71.
15. *Cao G. Z., Schermer J. J., van Enckevort W. J. P. et al.* Growth of {100} textured diamond films by the addition of nitrogen // J. Appl. Phys. – 1996. – **79**. – P. 1357–1364.
16. *Jiang X., Jia C. L.* The coalescence of [001] diamond grains heteroepitaxially grown on (001) silicon // Appl. Phys. Lett. – 1996. – **69**. – P. 3902–3904.
17. *Gruen D. M.* Nanocrystalline diamond films // Ann. Rev. Mater. Sci. – 1999. – **29**. – P. 211–259.
18. *Spitsyn B., Bouilov L. L, Deryagin B. V.* Vapor growth of diamond on diamond and other surfaces // J. Cryst. Growth. – 1981. – **52**. – P. 219–226.
19. *Kamo M., Sato Y., Matsumoto S., Setaka N.* Diamond synthesis from gas phase in microwave plasma // Ibid. – 1983. – **62**. – P. 642–644.
20. *Afzal A., Rego C. A., Ahmed W., Cherry R. I.* HFCVD diamond grown with added nitrogen: film characterization and gas-phase composition studies // Diamond Relat. Mater. – 1998. – **7**. – P. 1033–1038.
21. *Handbook* of Industrial Diamonds and Diamond Films / Eds. M. A. Prelas, G. Popovichi, L.K. Bigelow. – New York: Marcel Dekker, 1998.
22. *Yan C. S.* Multiple twinning and nitrogen defect center in chemical vapor deposited homoepitaxial diamond // Ph. D. Dissertation. – Birmingham: University of Alabama, 1999.
23. *Yan C. S., Vohra Y. K.* Multiple twinning and nitrogen defect center in chemical vapor deposition deposited homoepitaxial diamond // Diamond Relat. Mater. – 1999. – **8**. – P. 2022–2031.
24. *Tamor M., Everson M. P.* On the role of penetration twins in the morphological development of vapor–grown diamond films // J. Mater. Res. – 1994. – **9**. – P. 1839–1847.
25. *Wild C., Kohl R., Herres N. et al.* Oriented CVD diamond films: twin formation, structure and morphology // Diamond Relat. Mater. – 1994. – **3**. – P. 373–381.
26. *Hemawan K. W., Yan C. S., Liang Q. et al.* Hot spot formation in microwave plasma CVD diamond synthesis // IEEE Trans. Plasma Sci. – 2011. – **39**. – P. 2790–2791.
27. *Meng Y. F., Yan C. S., Mao H. K., Hemley R. J.* Enhanced optical properties of chemical vapor deposited single crystal diamond by low-pressure high-temperature annealing // Proc. Nat. Acad. Sci. – 2008. – **105**. – P. 17620–17625.
28. *Liou Y., Inspektor A., Weimer R. et al.* The effect of oxygen in diamond deposition by microwave plasma enhanced chemical vapour deposition // J. Mater. Res. – 1990. – **5**, N 11. – P. 2305–2312.
29. *Fuchs F., Wild C., Schwarz K. et al.* Hydrogen-induced vibrational and electronic transitions in chemical vapor deposited diamond, identified by isotopic substitution // Appl. Phys. Lett. – 1995. – **66**. – P. 177–179.

30. *Tallaire A., Achard J., Silva F. et al.* Oxygen plasma pre-treatments for high quality homoepitaxial CVD diamond deposition // Phys. Stat. Sol. A. – 2004. – **241**, N 10. – P. 2419–2424.
31. *Martineau P. M., Lawson S. C., Lawson A. J. et al.* Identification of synthetic diamond grown using chemical vapor deposition (CVD) // Gems Gemol. – 2004. – **40**. – P. 2–25.
32. *Smith C. P., Bosshart G., Ponahlo J. et al.* GE POL diamonds: before and after // Ibid. – 2000. – **36**. – P. 192–215.
33. *Weerdt F. D., van Royen J.* Investigation of seven diamonds HPHT treated by NovaDiamond // J. Gemm. – 2000. – **7**. – P. 201–208.
34. *Shiryaev A. A., Hutchison M. T., Dembo K. A. et al.* High temperature–high pressure annealing of diamond small angle X-ray scattering and optical study // Physica B. – 2001. – **308**–**310**. – P. 598–603.
35. *Collins A. T., Connor A., Ly C.-H. et al.* High-temperature annealing of optical centers in type I diamond // J. Appl. Phys. – 2005. – **97**, N 8, art. 083517.
36. *Weerdt F. D., Collins A. T.* HPHT annealing of natural diamond, new diamond and frontier // Carbon Technology. – 2007. – **17**, N 2. – P. 91–103.
37. *Charles S. J., Butler J. E., Feygelson B. N. et al*. Characterization of nitrogen-doped chemical vapor deposited single crystal diamond before and after high pressure, high temperature annealing // Phys. Stat. Sol. – 2004. – **242**. – P. 2473–2485.
38. *Woods G. S., Collins A. T.* Infrared absorption spectra of hydrogen complexes in type I diamonds // J. Phys. Chem. Solids. – 1983. – **44**. – P. 471–475.
39. *Glover C., Newton M. E., Martineau P. et al*. Hydrogen incorporation in diamond: the nitrogen-vacancy-hydrogen complex // Phys. Rev. Lett. – 2003. – **90**, art. 185507.
40. *Novikov N. V., Sirota Yu. V., Mal'nev V. I., Petrusha I. A.* Mechanical properties of diamond and cubic BN at different temperatures and deformation rates // Diamond Relat. Mater. – 1993. – **2**. – P. 1253–1256.
41. *Drory M. D., Dauskardt R. H., Kant A., Ritchie R. O.* Fracture of synthetic diamond // J. Appl. Phys. – 1995. – **78**. – P. 3083–3088.
42. *Novikov N. V., Dub S. N.* Hardness and fracture toughness of CVD diamond film // Diamond Relat. Mater. – 1996. – **5**. – P. 1026–1030.
43. *Yan C. S., Mao H. K., Li W. et al.* Ultrahard single crystal diamond from chemical vapor deposition. – Phys. Stat. Sol. (a). – 2004. – **201**. – P. 25–27.
44. *Liang Q., Yan C. S., Meng Y. et al.* Recent advances in high-growth rate single-crystal CVD diamond // Diamond Relat. Mater. – 2009. – **18**. – P. 698–703.
45. *Liang Q., Yan C. S., Meng Y. et al.* Enhancing the mechanical properties of CVD single crystal diamond // J. Phys. Condens. Matt. – 2009. – **21**, N 36, art. 364215.
46. *Novikov N. V., Dub S. N, Mal'nev V. I.* High-temperature fracture toughness of monocrystalline diamonds // J. Hard. Mater. – 1993. – **4**. – P. 19–27.
47. *Patridge G. P., May P. W., Rega C. A., Ashfald M. N. R.* Potential for diamond fibres and diamond fibre composites // Mat. Sci. Tech. – 1994. – **10**. – P. 505–512.
48. *Locher R., Wild C., Herres N. et al.* Nitrogen stabilized <100> texture in chemical vapor deposited diamond films // Appl. Phys. Lett. – 1994. – **65**. – P. 34–36.
49. *Burns R. C., Cvetkovic V., Dodge C. N. et al.* Growth-sector dependence of optical features in large synthetic diamonds // J. Cryst. Growth. – 1990. – **104**. – P. 257–279.
50. *Ramamurti R., Becker M., Schuelke T. et al.* Boron-doped diamond deposited by microwave plasma-assisted CVD at low and high pressures // Diamond Relat. Mater. – 2008. – **17**. – P. 481–485.
51. *Tsuno T., Tomikawa T., Shikata S. et al.* Diamond (001) single-domain 2×1 surface grown by chemical vapor deposition // Appl. Phys. Lett. – 1994. – **64**. – P. 572–574.
52. *Anderson G. C., Prawer S., Johnston P., McCulloch D.* The effect of carbon and nitrogen implantation on the abrasion resistance of type IIa (110) diamond // Nucl. Instrum. Meth. Phys Res. B. – 1993. – **80**–**81**. – P. 1451–1455.
53. *Pat. 6322891 US, IPC C01B31/06, C09K3/14, C30B29/04*. Thermally-diffused boron diamond and its production / Y. Meng, T. R. Anthony. – Publ. 27.11.01.
54. *Anthony T. R.* Stresses generated by impurities in diamond // Diamond Relat. Mater. – **4**. – P. 1346–1352.
55. *Larson B. C., Yang W., Ice G. E. et al.* Three-dimensional X-ray structural microscopy with submicrometer resolution // Nature. – 2002. – **415**, N 6874. – P. 887–890.
56. *Weir C. E., Lippincott E. R., Van Valkenburg A., Bunting E. N.* Infrared studies in the 1-micron to 15-micron region to 30,000 atmospheres // J. Res. Nat. Bur. Stand. Sec. A: Phys. Chem. – **63**. – 1959.

57. *Hemley R. J., Ashfold M. N.* The revealing role of pressure in the condensed matter sciences // Phys. Today. – 1998. – **51**. – P. 26–32.
58. *Hemley R. J.* A pressing matter // Phys. World. – 2006. – **19**. – P. 26–30.
59. *Goncharov A. F., Hemley R. J., Mao H. K., Shu J.* New high-pressure excitations in parahydrogen // Phys. Rev. Lett. – 1998. – **80**. – P. 101–104.
60. *Merkel S., Hemley R. J., Mao H. K.* Finite element modeling of diamond deformation at multimegabar pressures // Appl. Phys. Lett. – 1999. – **74**, N 5. – P. 656–658.
61. *Takano K. J., Wakatsuki M.* An Optical high-pressure-cell with spherical sapphire anvils // Rev. Sci. Instrum. – 1991. – **62**. – P. 1576–1580.
62. *Xu J., Mao H., Hemley R. J., Hines E.* Large volume high-pressure cell with supported moissanite anvils // Ibid. – 2004. – **75**. – P. 1034–1038.
63. *Mao H. K., Hemley R. J.* Ultrahigh-pressure transitions in solid hydrogen // Rev. Modern Phys. – 1994. – **66**. – P. 671–692.
64. *Dewaele A., Loubeyre P., Andre R., Hartwig J.* An X-ray topographic study of diamond anvils: correlation between defects and helium diffusion // J. Appl. Phys. – 2006. – **99**, art. 104906.
65. *Hemley R. J., Mao H.-K., Goncharov A. F. et al.* Synchrotron infrared spectroscopy to 0.15 eV of h-2 and d-2 at megabar pressures // Phys. Rev. Lett. – 1996. – **76**. – P. 1667–1670.
66. *Hemley R. J., Mao H. K.* Progress in cryocrystals at megabar pressures // J. Low Temp. Phys. – 2001. – **122**. – P. 331–344.
67. *Gregoryanz E., Goncharov A. F., Matsuishi K. et al.* Raman spectroscopy of hot dense hydrogen // Phys. Rev. Lett. – 2003. – **90**, art. 175701.
68. *Mills R. L., Liebenberg D. H., Bronson J. C., Schmidt L. C.* Procedure for loading diamond cells with high-pressure gas // Rev. Sci. Instrum. – 1980. – **51**. – P. 891–895.
69. *Eremets M. I.* Megabar high-pressure cells for Raman measurements // J. Raman Spectr. – 2003. – **34**. – P. 515–518.
70. *Sun L., Ruoff A. L., Stupian G.* Convenient optical pressure gauge for multimegabar pressures calibrated to 300 GPa // Appl. Phys. Lett. – 2005. – **86**, art. 014103.
71. *Zha C. S., Krasnicki S., Meng Y. F. et al.* Composite chemical vapor deposition diamond anvils for high-pressure/high-temperature experiments // High Pressure Research. – 2009. – **29**. – no. 3. – P. 317–324.
72. *Wang S., Meng Y., Ando N. et al.* Single-crystal CVD diamonds as small-angle X-Ray scattering windows for high-pressure research // J. Appl. Crystallogr. – 2011. – **45**. – P. 453–457.
73. *Ando N., Chenevier P., Novak M. et al.* High hydrostatic pressure small-angle X-ray scattering cell for protein solution studies featuring diamond windows and disposable sample cells // Ibid. – 2008. – **41**. – P. 167–175.
74. *Shiryaev A. A.* SANS from defects in diamond // Ibid. – 2007. – **40**. – P. s116–s120.
75. *Shiryaev A. A., Boesecke P.* Small-angle X-ray and neutron scattering from diamond single crystals. – http://arxiv.org/abs/1110.6270, 2011.
76. *Gaukroger M. P., Martineau P. M., Crowder M. J. et al.* X-ray topography studies of dislocations in single crystal CVD diamond // Diamond Relat. Mater. – 2008. – **17**. – P. 262–269.
77. *Popov D.* Personal Communication, 2012.
78. *Ando N., Barstow B., Baase W. et al.* Structural and thermodynamic characterization of T4 lysozyme mutants and the contribution of internal cavities to pressure denaturation // Biochem. – 2008. – **47**. – P. 11097–11109.

Carnegie Institution of Washington,
Geophysical Laboratory

Received 28.09.2012

HPCAT, Geophysical Laboratory,
Carnegie Institution of Washington,
Advanced Photon Source,
Argonne National Laboratory

HPSynC, Geophysical Laboratory,
Carnegie Institution of Washington,
Advanced Photon Source,
Argonne National Laboratory